Feasibility of using 3D CZT drift strip detectors for small Compton camera space missions

Owe, S.R.H.; Kuvvetli, I.; Zoglauer, A.; Budtz-Jørgensen, C.

Published in:
Journal of Instrumentation

Link to article, DOI:
10.1088/1748-0221/19/01/C01005

Publication date:
2024

Document Version
Publisher's PDF, also known as Version of record

Journal of Instrumentation

PAPER • OPEN ACCESS

Feasibility of using 3D CZT drift strip detectors for small Compton camera space missions

Published by IOP Publishing for Sissa Medialab

Received: *September 28, 2023*
Revised: *November 19, 2023*
Accepted: *November 20, 2023*
Published: *January 5, 2024*

24th International Workshop on Radiation Imaging Detectors
Oslo, Norway
25–29 June 2023

Feasibility of using 3D CZT drift strip detectors for small Compton camera space missions

S.R.H. Owe,[a,*] **I. Kuvvetli,**[a] **A. Zoglauer**[b] **and C. Budtz-Jørgensen**[a]

[a] *DTU Space, Technical University of Denmark,*
Elektrovej building 327, 2800 Kgs. Lyngby, Denmark
[b] *Space Sciences Laboratory, University of California, Berkeley,*
7 Gauss Way, Berkeley, CA 94720, U.S.A.

E-mail: shoowe@space.dtu.dk

Abstract: This feasibility study explores the possibility of using 3D CZT drift strip detectors developed by DTU Space in a small Compton camera payload, with the primary objective of technology demonstration. We have defined a scalable mass model for the payload, comprising eight 3D CZT drift strip detectors surrounded by CsI scintillator detectors for active shielding. The payload's angular resolution, effective area, and efficiency are evaluated through simulations of far-field monochromatic point sources. The instrument's sensitivity is assessed in a low Earth orbit background environment for nuclear line and continuum emission sources. With a 3σ point source sensitivity in the order of 10^{-4} [ph/cm^2/s], it is evident that such an instrument only allows for limited scientific goals. In-orbit simulations of bright sources are conducted, resulting in reasonable observation times for the Crab Nebula at a 5σ significance level. Furthermore, in-orbit simulations of a selection of bright gamma-ray bursts indicate the potential for observing bright transient events. The study underscores the potential of using 3D CZT drift strip detectors in Compton camera configurations but also highlights the need for a larger effective area to improve sensitivity. However, for a technology demonstration aimed at increasing the Technology Readiness Level of the 3D CZT drift strip detector, a small Compton camera configuration like the one presented in this study could be a viable solution.

Keywords: Space instrumentation; X-ray detectors and telescopes; Gamma detectors; Instrument optimisation

*Corresponding author.

https://doi.org/10.1088/1748-0221/19/01/C01005

Contents

2024 JINST 19 C01005

1 Introduction

The low-to-medium-energy gamma-ray range (0.1 to 100 MeV) is one of the least explored in the electromagnetic spectrum. It is inherently difficult to observe due to low flux, low interaction probability, three energy loss processes, and a high background radiation rate. Nevertheless, a wide range of interesting astrophysical processes can be studied in this energy band. Examples include nuclear lines from radioactive nuclei generated by supernova explosions, short gamma-ray bursts from colliding neutron stars, 511 keV gamma-rays from electron-positron annihilation, and gamma-ray emissions from the most energetic environments in our universe, such as those around pulsars or accreting black holes. Only the next generation of space telescopes will be capable of making meaningful advances in this field. To enhance the sensitivity of future observatories, new state-of-the-art sensor technology will be a key contributor. For a detector to be selected to fly on any future large observatory, it must undergo thorough testing and have a high Technology Readiness Level (TRL). This simulation study investigates the feasibility of operating a small spaceborne Compton camera payload utilizing the 3D CdZnTe (CZT) drift strip detector technology.

1.1 The 3D CZT drift strip detector

The detector group at DTU Space initiated a development program aimed at improving the spectral performance of CZT detectors. This effort resulted in the creation of the 3D CZT drift strip detector [1–3]. This detector uses a unique electrode geometry, where anodes are screened from the poor hole movement in CZT. Thin anode strips, separated by negatively biased drift strips, ensure the drift of electrons to an anode. On the opposite side, segmented cathode strips are present. This

unique electrode geometry allows for the use of distinctive spatial position algorithms [4] and makes the detector primarily dependent on the electron charge transport. Recent prototypes, measuring 2×2×0.5 cm^3, have achieved sub-millimeter position resolution (<0.5 mm @ 662 keV) in 3D and demonstrated excellent energy resolution (at best <1% @ 662 keV) [4–7]. It was demonstrated that the spatial positioning algorithm could be extended to identify Compton interactions within the same detector volume. Some issues can occur when assigning the photon interaction coordinates, and the algorithms do not currently include interactions collected by the same anode in the detector. However, despite the shortcomings, a single detector crystal can be operated as a Compton camera [5]. This is especially favorable for space applications where low source fluxes require the identification of as many gamma-ray interactions as possible. In recent years, the technology has matured significantly, and state-of-the-art 3D CZT drift strip detector modules can now achieve sizes of 4×4×0.5 cm^3. Characterization results of these modules are ongoing and will be published elsewhere.

The 3D CZT drift strip detector technology is applicable in various fields, such as medical applications [7] and space [5]. The TRL of the 3D CZT drift strip detector technology has increased since its invention, advancing from a TRL of 1 to 4. Proof of concept studies and relevant tests have been conducted in a laboratory environment. To further elevate the TRL, the technology must be assessed in a relevant environment, namely, in space. One viable approach is to deploy the detector technology in a small Compton camera, either on a CubeSat or another small satellite payload. In this study, we investigate the feasibility of conducting astronomical observations in a low Earth orbit (LEO) environment using a CubeSat-sized payload of 3D CZT drift strip detectors operated as a Compton camera.

2 Model setup

To evaluate the detection capabilities of a simple Compton camera concept utilizing 3D CZT drift strip detectors in a space radiation environment such as LEO, we make use of Monte Carlo simulations using the Medium-Energy Gamma-ray Astronomy library (MEGAlib) [8]. In this section we introduce the simulation framework, together with the instrument model, and simulation method for this study.

2.1 Simulation framework

The software package MEGAlib,[1] incorporates ROOT and Geant4 and specializes in simulating Compton telescopes. It comprises all necessary steps, including simulation, event reconstruction, image reconstruction, and data analysis. The instrument mass model is defined using the MEGAlib tools, along with explicit detector specifications that allow the application of realistic detector effects such as energy and positions resolution, thresholds, etc. The sources (both astrophysical and background) used for the Monte Carlo simulations are also defined using the framework. In addition, all necessary data analysis tools for the study are provided with MEGAlib.

2.2 Instrument model

Compton cameras typically operate in the 0.1–10 MeV range and utilize one or more Compton scatter interactions in the detectors to identify the origin of the photon. By measuring the position

[1]MEGAlib: https://github.com/zoglauer/megalib.

2024 JINST 19 C01005

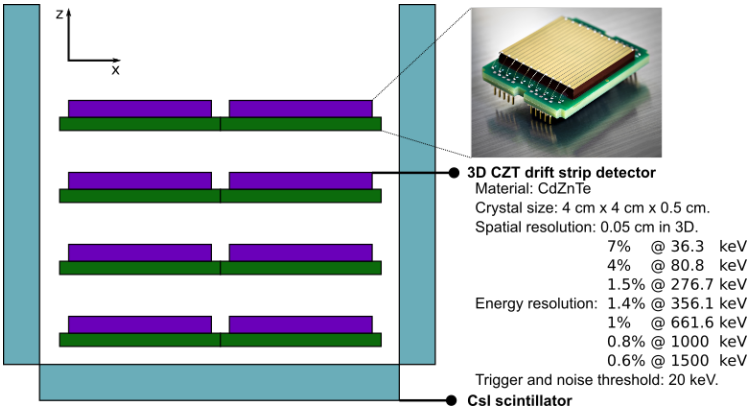

Figure 1. Illustration of the instrument mass model consisting of eight 3D CZT drift strip detectors surrounded by 1 cm thick CsI scintillator active shielding. Zenith axis is defined by the z-axis.

and energy deposited by several Compton interactions within the camera, it is possible to reconstruct the source position to a cone in the sky. Several interactions, and overlapping cones can then with image reconstruction reveal the source location [9].

A mass model of a compact Compton camera based on 3D CZT drift strip detectors was developed with MEGAlib. Figure 1 shows a schematic of the payload geometry and detector specifications. Final characterization work of the latest detector module ($4\times4\times0.5\,\mathrm{cm}^3$) is ongoing, therefore specifications of the detector in MEGAlib is based on previous detector version performances. The energy resolution is extracted from [10] and set to twice the FWHM for a conservative value. In reality, with good electronics, these values could improve further. We chose to restrict the number of CZT detectors in the camera to eight. This resulted in four layers with two detectors each, and a distance of 1.1 cm between the layers. The eight CZT detectors are surrounded by 1 cm-thick CsI scintillators, used as active shielding. Active shielding and background rejection is a crucial element when building a Compton camera for LEO, due to high background in the Compton-regime. The mass model of the instrument is kept as simple as possible for this feasibility study. That excludes photomultipliers connected to the scintillator shields, other passive material in the instrument, and spacecraft specific materials. Thus, we only include the most basic parts of the payload.

Since we wish to measure Compton sequences from astrophysical sources occurring in the CZT detector payload, we define two trigger criteria. The first one states that two (or more hits) in any CZT detector trigger the system and the event is stored. This includes two or more interactions in a single CZT detector or two or more interactions in different detectors. The second trigger criteria states that if an interaction occurs in the scintillator shield at the same time as in the CZT, the event is vetoed. In LEO, these are predominantly upward moving Earth-albedo photons, i.e., background. The shield also vetoes a significant fraction of charged particle events. As consequence, only Compton sequences exclusively occurring in the 3D CZT drift strip detectors are kept.

2.3 Method

The chronology of the simulation is as follows: first, the geometry and detector characteristics are specified in MEGAlib. This includes the previously defined mass model, along with detector type, material, resolutions, and trigger criteria for the system. Next, simulations are conducted with

2024 JINST 19 C01005

the instrument payload observing a specific source. Finally, the MEGAlib tools are employed to reconstruct the Compton sequences, generate images, and analyze the simulated data. Since the chronological order of the interactions is unknown, Compton sequence reconstruction is required to determine the path in the detector. We only consider Compton sequences with 2–7 interactions, and with a minimum distance of 1.6 mm (in 3D) in between any interaction. The minimum distance of 1.6 mm was chosen, since it corresponds to the anode pitch in the 3D CZT drift strip detector.

Four source types are defined for this study: nuclear lines, continuum emission, transients, as well as the associated background. Sources are specified in MEGAlib with location, flux, energy range, and spectral type. Simulations for a range of monoenergetic far-field point sources (200 keV–2000 keV) are used to evaluate the overall instrument performance, and to assess basic payload performance parameters such as effective area, Angular Resolution Measure (ARM), and efficiency for a range of monochromatic energies. To evaluate the sensitivity (minimum detectable flux) of the instrument, the background environment is an essential factor. The background in-orbit simulation is based on data retrieved from Spenvis,[2] for an orbit like that of the NuSTAR satellite (altitude: 575 km, inclination: 6 degrees). The background source files are generated using MEGAlib and include photonic, leptonic, and hadronic components. We assume the instrument to be off during South Atlantic Anomaly (SAA) passages, and therefore we do not include the trapped hadronic contribution. The simulation does not yet take into account the activation build-up in the instrument, thus the background simulation reflects the beginning of the observation period.

To assess payload sensitivity, S, for a given significance, z, for a point source, the following expression is used [9]

$$S = \frac{z\sqrt{N_S + N_B}}{A_{\text{eff}} T_{\text{eff}}}, \tag{2.1}$$

where N_S is the measured source counts in the source extraction region (3σ ARM), N_B is the measured background counts in the source extraction region, A_{eff} is the effective area of the instrument, and T_{eff} is the effective observation time. The minimum detectable flux can be expressed (given the number of source photons at the sensitivity limit $N_S = S T_{\text{eff}} A_{\text{eff}}$, and solving eq. (2.1) for S) by

$$S = \frac{z^2 + z\sqrt{z^2 + 4N_B}}{2T_{\text{eff}} A_{\text{eff}}}. \tag{2.2}$$

This equation can be used to evaluate the payload sensitivity (narrow-line and continuum) in a given background environment.

To finally evaluate the feasibility of operating the 3D CZT drift strip detectors in a payload in space, we conclude the study with simulations of known astronomical sources. We investigate a continuum source (the Crab), and transient sources, with a selection of bright Gamma Ray Bursts (GRBs).

3 Payload performance

In the following sections, we present the simulation results of this study. First, we present the basic payload performance parameters. Next, through a long background environment simulation, we extract the background components to assess payload sensitivity. Finally, we assess the instrument's performance when observing known astronomical sources (both continuum and transient) in a LEO space radiation environment.

[2] Spenvis: https://www.spenvis.oma.be/.

2024 JINST 19 C01005

3.1 Basic performance

Simulations of far-field point sources with monoenergetic beams are used to evaluate the ARM, effective area, and efficiency of the instrument. An energy window of $\Delta E = \pm 2\sigma$ is used, and a 3σ ARM window is additionally employed to evaluate effective area and efficiency. Thus, we exclusively consider data within the photopeak domain of the source resolution element.

In figure 2(left) the simulated effective area as a function of energy is shown. The effective area was evaluated at a selection of energies at different polar angles (θ, ϕ), varying θ from 0° to 80°, with $\phi = 0$. Zenith is defined along the z-axis in figure 1, where θ starts from the positive z-axis (zenith), and ϕ from the positive x-axis. The effective area peaks at 300 keV and experiences a steady drop hereafter. This is expected due to the small number of detectors. Including more detector material will increase the stopping power, and by that increase effective area at higher energies. We see the effective area, especially for the lower energies, being strongly affected by the zenith angle of the source, and it peaks around $\theta = 10°$. As the zenith angle increases, the exposed geometrical surface initially increases, resulting in an increase in effective area. Later on, the effective area will decrease once again as the angle further increases, due to increased probability of absorption in the CsI shields. The effects are not as visible at higher energies, where the stopping power limits the effective area.

Figure 2(middle) shows the ARM as a function of energy at zenith incidence angle. The instrument consist of CZT detectors, and Doppler broadening therefore imposes a limiting factor on the ARM [12]. In addition, the lower the energy, the closer the interactions are, and therefore, the relative position uncertainty between detector position resolution of 0.5 mm and a minimum distance of 1.6 mm between interactions also limits the ARM.

Figure 2(right) shows the efficiency of the instrument at zenith compared to that of COMPTEL [11]. The efficiency was calculated as the ratio between effective area and geometrical area. The efficiency of the instrument is comparable to that of COMPTEL around 1200 keV, but is less than that of COMPTEL at higher energies. Adjusting number of layers, event selection, and layer distance indicates the instrument could achieve larger efficiency.

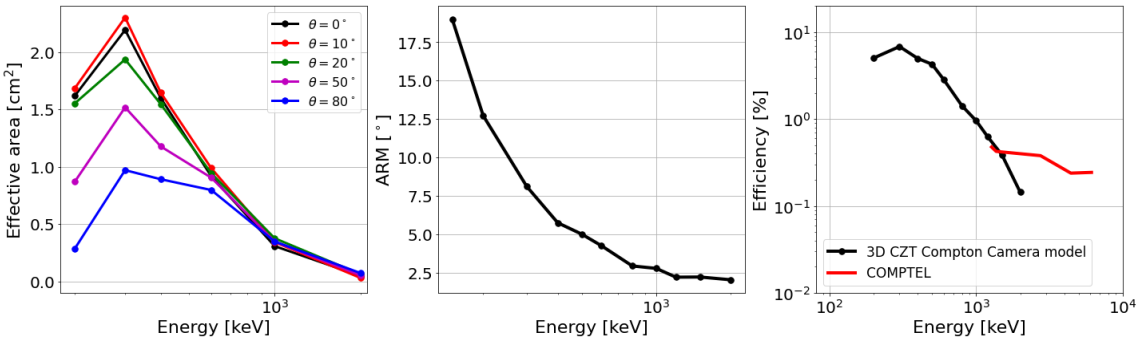

Figure 2. Basic performance parameters of the 3D CZT drift strip detector Compton camera. (Left) Effective area as a function of source energy. (Middle) ARM as a function of energy. (Right) Efficiency at zenith as a function of energy. COMPTEL efficiency is taken from [11].

2024 JINST 19 C01005

3.2 Sensitivity

The calculated narrow-line and continuum sensitivity of the instrument is given in table 1. Both are evaluated for 3σ significance, with an effective observation time of 10^6 s, using eq. (2.2).

For the narrow-line sensitivity of the payload model, we applied the effective area presented in figure 2 (left) at zenith. An energy window of $\Delta E = \pm 2\sigma$ was used. The continuum sensitivity of the payload model was evaluated with a power-law spectrum (E^{-2}), and the energy window for continuum sensitivity calculations was set to $\Delta E = E$. In both cases, we utilized simulations of the background environment to extract the background radiation rate measured by the payload for the specified energy and source extraction region. The calculated sensitivities are in the order of 10^{-4} ph/cm^2/s. This is not a good sensitivity, and in reality, we expect the numbers to be at least a factor of 2–3 worse when passive material and activations are included in the analysis. However, some limited science goals could be possible, especially just for the case of technology demonstration in space. The sensitivity is especially limited by the small effective area. Increasing the effective area of the payload, together with better background suppression, can result in an improvement of sensitivity.

Table 1. Instrument model sensitivity (3σ) calculated for an effective observation time of 10^6 s. The source extraction region is a 3σ ARM window. The narrow-line sensitivity energy window is $\Delta E = \pm 2\sigma$, and the continuum sensitivity energy window is $\Delta E = E$.

	Energy [keV]	3σ point source sensitivity [10^{-4}ph/cm^2/s]
Narrow-line	200	2.4
	400	1.3
	600	1.0
	1000	1.6
	2000	4.7
Continuum	150–450	9.1
	300–900	6.6
	450–1350	7.0
	750–2250	9.2
	1500–4500	20.0

3.3 Continuum source: the Crab

The sensitivity analysis of the instrument suggests that limited scientific objectives should be attainable. Therefore, it is valuable to investigate the payload's performance in an astronomical context, particularly when considering bright sources.

To assess the instrument's performance in observing a known continuum source, we chose the Crab Nebula. It is a bright source and serves as a standard candle within the gamma-ray community. The Crab is modeled using a power-law and was defined in MEGAlib in the energy range of 50–10000 keV, with spectral definition and flux as documented in [13]. With a simulation

2024 JINST 19 C01005

only including the Crab source, the ARM and effective area was determined in energy windows of $E = \Delta E$, and the source extraction region defined as 3σ ARM. Next, the required effective observation time for a 5σ observation was calculated using eq. (2.2). The background rate was extracted from a background-only simulation for the given energy and source extraction window. The resulting ARM, effective area, and effective observation time are summarized in table 2. We observe the shortest required observation time at 300 keV, where the Crab flux is higher, and the payload has a larger effective area. The observation times, ranging from approximately 1 to 8 hours, are reasonable for a small satellite mission like a technology demonstration. A simulation combining the Crab and in-orbit background sources ran for an observation time of 12 ks. The reconstructed images are displayed in figure 3. The background at 300 keV is notably more suppressed compared to 600 keV, thanks to the shorter observation times required at 300 keV to achieve a significant Crab signal.

Table 2. In-orbit payload ARM, effective area, and effective observation time of the Crab.

Energy [keV]	**ARM [°]**	**A_{eff} [cm^2]**	**T_{eff} [s] (5σ)**
300	10.3	1.9	4103.8
600	5.7	1.6	10556.4
900	3.7	0.8	30285.3

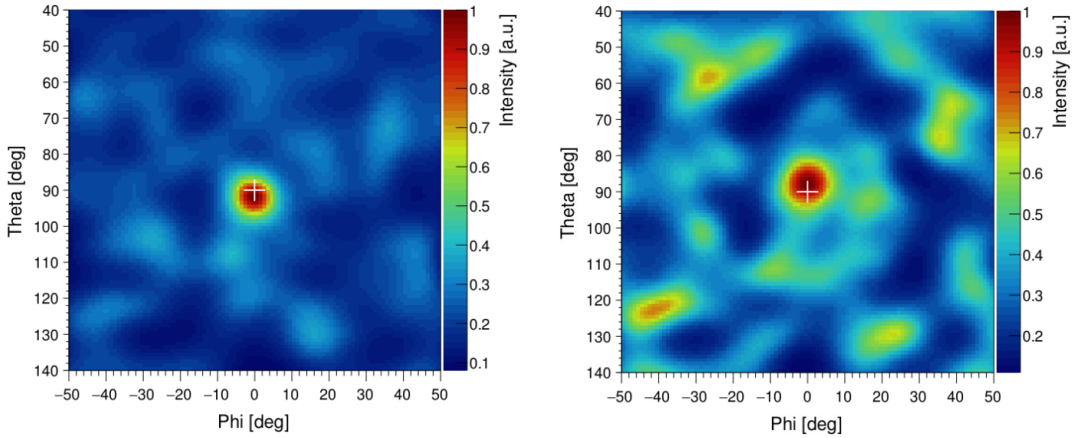

Figure 3. Simulation of an in-orbit observation of the Crab (12 ks at zenith) at 300 keV (left) and 600 keV (right) with an energy window of $\Delta E = E$. White crosses indicate the true source position.

3.4 Transient source: gamma-ray burst

GRBs are transient events in the sky, therefore, instruments with large fields of view are preferred for detecting GRBs. Short GRBs (< 2 s) are associated with compact binary system mergers, while long GRBs (> 2 s) are associated with core-collapse supernovae. Observing GRBs in coincidence with a gravitational wave signal is a key factor in multi-messenger astronomy. Several groups are exploring the development of CubeSats for GRB detection and localization to improve the chances of observation. Examples of current and future missions include Glowbug [14], BurstCube [15], and MoonBEAM [16].

2024 JINST 19 C01005

The spectral and fluence characteristics of GRBs vary greatly. GRBs with a small fluence will be impossible to detect given our low effective area. Therefore, we have selected a sample of six bright GRBs that are present in both the 'CGRO/BATSE Complete Spectral Catalog of Bright GRBs' [17] and the 'CGRO/BATSE 5B Gamma-Ray Burst Spectral Catalog' [18]. All GRBs were simulated in the previously mentioned background environment, with the GRB at zenith. In figure 4 the reconstructed images of the six simulated GRBs are shown. Four out of the six GRBs are visible in the image, with three distinctly visible above the background: GRB 990411, GRB 980923, and GRB 991127. GRB 980208 is also visible, albeit slightly off-axis from the true source position. The remaining two GRBs, 4B 940902 and 4B 930425, were not visible, primarily due to their lower fluence. This indicates that the instrument, designed for space qualification of the detector technology, could possibly detect bright GRBs if they occur within its field of view.

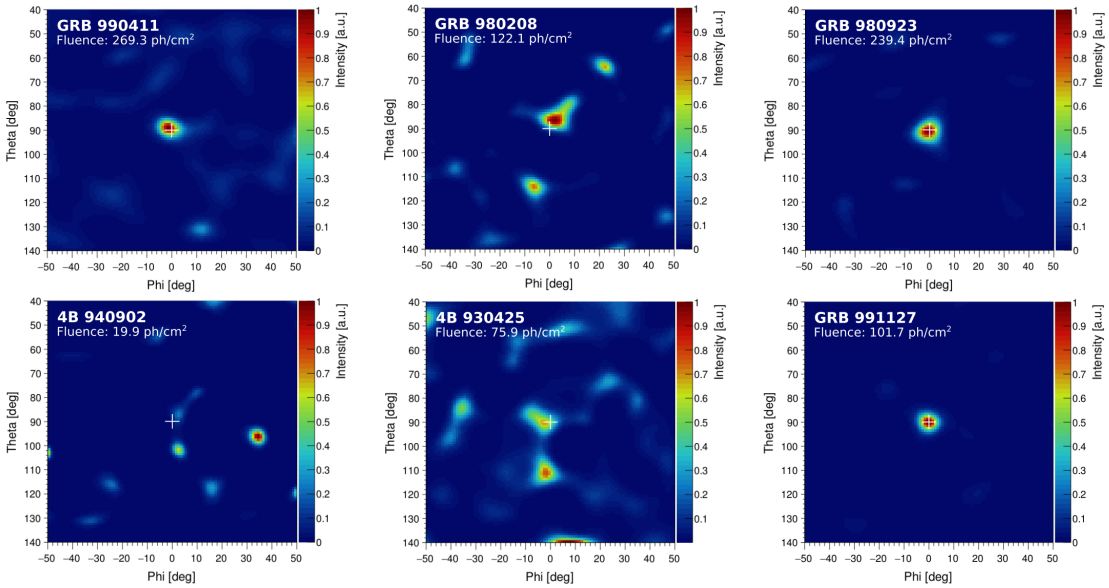

Figure 4. Simulation of six on-axis GRBs. The white cross indicates the true source position, and the GRB name and associated fluence are indicated in the upper left corner of each image.

4 Conclusion

The payload, consisting of eight 3D CZT drift strip detectors and CsI scintillator for active shielding, was evaluated through simulations for effective area, ARM, efficiency, and sensitivity. Due to its small size and the high background rate, the instrument has limited sensitivity, impacting achievable scientific goals. However, observing bright sources like the Crab Nebula and GRBs is feasible with relatively short observation times. This study establishes a baseline for the potential achievements of such an instrument, emphasizing scalability for optimization. It is crucial to note that these simulations represent a best-case scenario, and the inclusion of passive materials may decrease sensitivity. In conclusion, this study suggests that a small technology demonstration mission using 3D CZT drift strip detectors as a simple Compton camera could attain some limited science goals.

2024 JINST 19 C01005

References

[1] M. Van Pamelen and C. Budtz-Jørgensen, *Novel electrode geometry to improve performance of CdZnTe detectors*, *Nucl. Instrum. Meth. A* **403** (1998) 390.

[2] M. Van Pamelen and C. Budtz-Jørgensen, *CdZnTe drift detector with correction for hole trapping*, *Nucl. Instrum. Meth. A* **411** (1998) 197.

[3] I. Kuvvetli et al., *A 3D CZT high resolution detector for x-and gamma-ray astronomy*, *Proc. SPIE* **9154** (2014) 91540X.

[4] C. Budtz-Jørgensen and I. Kuvvetli, *New Position Algorithms for the 3-D CZT Drift Detector*, *IEEE Trans. Nucl. Sci.* **64** (2017) 1611.

[5] S. Owe et al., *Evaluation of a Compton camera concept using the 3D CdZnTe drift strip detectors*, vol. 14, IOP Publishing (2019) [DOI:10.1088/1748-0221/14/01/C01020].

[6] S. Owe, I. Kuvvetli and C. Budtz-Jørgensen, *Carrier Lifetime and Mobility Characterization using the DTU 3D CZT Drift Strip Detector*, *IEEE Trans. Nucl. Sci.* **68** (2021) 2440.

[7] S. Owe et al., *Evaluation of CZT Drift Strip Detectors for use in 3D Molecular Breast Imaging*, *IEEE Trans. Radiat. Plasma Med. Sci.* **7** (2023) 113.

[8] A. Zoglauer, R. Andritschke and F. Schopper, *MEGAlib — The Medium Energy Gamma-ray Astronomy Library*, *New Astron. Rev.* **50** (2006) 629.

[9] A.C. Zoglauer, *First Light for the next Generation of Compton and Pair telescopes*, Ph.D. Thesis, Technische Universität München (2005).

[10] I. Kuvvetli and C. Budtz-Jørgensen, *Pixelated CdZnTe drift detectors*, *IEEE Nucl. Sci. Symp. Conf. Rec.* **7** (2004) 4360.

[11] V. Schönfelder et al., *Instrument description and performance of the imaging gamma-ray telescope COMPTEL aboard the Compton Gamma-Ray Observatory*, *Astrophys. J. Suppl.* **86** (1993) 657.

[12] A. Zoglauer and G. Kanbach, *Doppler broadening as a lower limit to the angular resolution of next-generation compton telescopes*, *Proc. SPIE* **4851** (2003) 1302.

[13] P. Sizun et al., *The integral/spi response and the crab observations*, *ESA Spec. Publ.* **552** (2004) 815 [astro-ph/0406058].

[14] J.E. Grove et al., *Glowbug, a Low-Cost, High-Sensitivity Gamma-Ray Burst Telescope*, in the proceedings of the *71st Yamada Conference: Gamma-ray Bursts in the Gravitational Wave Era 2019*, Yokohama, Japan, 28 October–1 November 2019 (2020) [arXiv:2009.11959].

[15] J. Racusin et al., *BurstCube: A CubeSat for Gravitational Wave Counterparts*, arXiv:1708.09292.

[16] M.S. Briggs, *The Moon Burst Energetics All-sky Monitor (MoonBEAM) CubeSat, a Gamma-ray Burst Detector for Cislunar Orbit*, *AGU Fall Meeting Abstracts* **2020** (2020) SH040-06.

[17] Y. Kaneko et al., *The complete spectral catalog of bright batse gamma-ray bursts*, *AIP Conf. Proc.* **836** (2006) 133 [astro-ph/0601188].

[18] A. Goldstein et al., *The BATSE 5B Gamma-Ray Burst Spectral Catalog*, *Astrophys. J. Suppl.* **208** (2013) 21 [arXiv:1311.7135].

2024 JINST 19 C01005